Synthesis of nanoscale heterostructures comprised of metal nanowires, carbon nanotubes, and metal nanoparticles: Investigation of their structure and electrochemical properties

Nitin Chopra,[1,2,*] Junchi Wu,[1] Paaras Agrawal[3]

[1] *Metallurgical and Materials Engineering, Center for Materials for Information Technology (MINT), Box 870202, The University of Alabama, Tuscaloosa, AL 35401 USA*

[2] *Department of Biological Sciences, Box 870202, The University of Alabama, Tuscaloosa, AL 35401 USA*

[3] *NSF-REH, Northridge High School, 2901 Northridge Rd, Tuscaloosa, AL 35406 USA*

* Corresponding author. Tel: 205-348-4153; Fax: 205-348-2164; E-mail: nchopra@eng.ua.edu (N. Chopra)

ABSTRACT

One-dimensional nanoscale heterostructures comprised of multi-segment gold-nickel nanowires, carbon nanotube, and nickel nanoparticles were fabricated in a unique approach combining top-down and bottom-up assembly methods. Porous alumina template was utilized for sequential electro-deposition of gold and nickel nanowire segments. This was followed by chemical vapor deposition growth of carbon nanotubes on multi-segment gold-nickel nanowires, where nickel segment also acted as a carbon nanotube growth catalyst. The aligned arrays of these gold-nickel-carbon nanotube heterostructures were released from porous alumina template and then subjected to wet-chemical process to decorate with nickel/nickel oxide core/shell nanoparticles. X-ray diffraction, scanning electron microscopy, transmission electron microscopy, and Raman spectroscopy were utilized for morphology, interface, defect, and structure characterization. The electrochemical performance of these heterostructures was studied using cyclic voltammetry method and the specific capacitance of various heterostructures was estimated and compared.

Keywords: Nanowire, carbon nanotube, nanoparticles, heterostructures, microscopy, Raman spectroscopy, electrochemistry

1. Introduction

Multi-component nanomaterials can surpass the challenges of multi-functionality associated with single-component nanostructures, where the former will introduce synergistic effects by way of morphology, composition, and properties of individual component in nanoscale heterostructures [1,2]. Towards this end, metallic nanowire-carbon nanotube (CNT) heterostructures attract research attention because of their unique properties, controlled growth, and ability to self-assemble. For example, these multi-segment or axially heterostructured nanowires fabricated by deposition inside porous alumina (AAO) template can result in segment-specific hydrophillicity or hydrophobicity allowing for novel self-assembly route [3]. In regard to growth control, both nanowires and CNTs can be grown on desired substrates with controlled sizes and spatial arrangements [4-6]. In this regard, AAO is also a suitable hard template route that allows for both diameter and site density (number of nanowires/CNTs per unit area) control depending upon the pore size and density of AAO. This approach has a potential to combine multiple processing steps to integrate metal nanowires with CNTs.

One dimensional metal-CNT heterojunctions with Ohmic or Schottky current-voltage (*I-V*) characteristic are building blocks in devices, as planar metal-semiconductor heterojunctions are building blocks in microelectronics [7]. A report demonstrates synthesis of ordered vertical arrays of nickel (Ni)-multiwalled CNT (MWCNT)-amorphous CNT (*a*-CNT) heterojunctions, which consist of a Ni nanowire, a MWCNT, and an *a*-CNT connected end to end (axial heterostructure), where the MWCNT is semiconducting and two Schottky contacts exist at the two ends of the MWCNT [8]. The *I-V* characteristics of the heterojunctions embedded in the arrays were measured and analyzed by a conductive AFM. It was observed that the Schottky contacts in the heterojunctions resulted in rectifying *I-V* characteristics.

CNTs have been used as electrodes for supercapacitors because of their excellent electrical properties and high surface areas [9,10]. However, CNT based supercapacitors have their own problems [11]. One of the major issues is the high contact resistance between the electrode and the current collector which limits their performance [10]. This contact resistance could be lowered by growing CNTs directly onto a conductive substrate, which can act as a current collector. Thus a hybrid metal-CNT heterostructure may reduce the contact resistance. A recent work shows the fabrication of ultra-high power supercapacitors by using multi-segmented CNT-Au nanowire structures as electrode, where both the CNT electrode and current collectors (Au nanowires) are integrated into an axially-heterostructured system [12].

While CNT can store energy as electrochemical double layer capacitor, another type of supercapacitors called redox supercapacitor or pseudo-capacitor, which utilizes reversible Faradaic-type charge transfer for charge/discharge process, has also been extensively investigated [13]. Nickel oxide (NiO) is a good candidate for surface redox reactions due to its high specific capacity, low cost, and good environmental compatibility [14]. However, the high resistivity of NiO electrodes is a serious drawback to their practical applications to supercapacitors [15]. An approach to improve the performance of NiO electrode is to combine carbon materials (double-layer capacitor) and NiO (pseudo-capacitor) as supercapacitor [15,16]. Herein, we reported the fabrication of three different nanocomposites consisting of Au/Ni nanowires (NWs), nanowires with CNTs (NW-CNT heterostructures), and nanowires and CNTs decorated with Ni/NiO core/shell nanoparticles (NW-CNC heterostructures), respectively. The multi-segment nanowires were prepared by electrodeposition in AAO template, CNTs were grown on nanowires within AAO templates in a CVD method, and Ni nanoparticles were nucleated onto heterostructures in a wet chemical method. This multi-step process of fabricating complex metal nanowire-CNT-

nanoparticle heterostructures is easy to control and suitable for production in large quantity. The produced nanostructures or heterostructures at each step of fabrication were thoroughly studied for their morphology, size, structure, and interfaces using microscopic and spectroscopic methods. The capacitances of the produced nanostructures and heterostructures was compared and analyzed using cyclic voltammetry (CV) measurement.

2. Experimental Section

2.1. Material and Methods

Nickel sulfate hexahydrate ($NiSO_4 \cdot 6H_2O$) was purchased from Mallinckrodt Baker, Inc. (New Jersey). Gold (I) potassium cyanide, ($KAu(CN)_2$), Sodium hydrogen carbonate ($NaHCO_3$, 99.7~100.3%), and Tri-n-octylphosphine oxide (TOPO, 98%) were bought from Alfa Aesar (Ward Hill, MA). Sodium hydroxide (NaOH) and Sodium Chloride (NaCl) were purchased from Fisher Scientific (New Jersey). Potassium hydroxide (KOH) was bought from Acros Organics (New Jersey). Nickel acetate tetrahydrate ($(CH_3CO_2)_2Ni \cdot 4H_2O$, 98%), Oleylamine ($C_{18}H_{37}N$), and Trioctylphosphine (TOP, 90%) were purchased from Sigma-Aldrich (St. Louis). All chemicals were used without further purification. Labnet centrifuge (Edison, NJ) was used to wash and separate samples. Before characterization, samples were dried and stored in a VWR vacuum oven (West Chester, PA). DI water (18.0 MΩ-cm) was obtained from a Barnstead International DI water system (E-pure D4641). Electrodeposition was performed using electrochemical workstation Parastat2273 (Princeton Applied Research). CNT growth processes were conducted in a Lindberg blue 3-zone tube furnace (Watertown, WI).

2.2. Synthesize Multi-Segment Metal Nanowires (NWs)

A thin layer of Au/Ag (~45 nm thick) was sputtered on the back side of porous alumina (AAO, pore size ~200nm) as the conductive part of working electrode. The working electrode was connected with electrochemical station using copper wire and silver paint. Au nanowires were potentiostatistically deposited from 0.02 M gold potassium cyanide in pH=10.0 $NaHCO_3$/NaOH buffer solution, while Ni nanowires were potentiostatistically deposited using sulfate solution with boric acid adjusting pH. Two-segment nanowires (Au/Ni nanowires or also referred as "NWs") were obtained by subsequently deposition of each segment from the corresponding electrolyte. The whole processes were performed at room temperature. After electro-deposition, AAO template with nanowires were washed with DI water and dried in vacuum oven.

2.3. Carbon Nanotube (CNT) Growth on Nanowires (NW-CNT heterostructures)

After reducing oxidized Ni in hydrogen, CNTs were grown on the tip of Au-Ni nanowires in a CVD process, involving xylene as a carbon source. Pure xylene precursor was injected through a syringe injector into a pre-heated zone for ~2 min and subsequently transported into the reaction zone (~ 700 °C) inside the quartz tube furnace. The xylene flow rate was reduced to 5 mL/h when H_2 in Ar carrier gas was introduced in the CVD reactor, where H_2 acted as an oxygen scavenger. The CVD reaction was continued for 1 h, after which H_2 and xylene flow was discontinued and furnace was cooled down under Ar flow. After the growth of CNT, AAO template was removed away by 3 M KOH, the obtained NW-CNT heterostructures were washed with DI water and stored in vacuum oven for the next step.

2.4. Nucleation of Ni Nanoparticles on NW-CNT Heterostructures (NW-CNC heterostructures)

The NW-CNT heterostructures were decorated with Ni nanoparticles through a direct nucleation process [17]. After being removed from AAO template, the brush-like NW-CNT heterostructures were pre-mixed with nickel acetate and oleylamine in a three-neck round bottom flask. The mixture was heated in ~90 ^{o}C oil bath under N_2 atmosphere for 40 min, followed by adding TOPO and TOP as stabilizer for Ni nanoparticle nucleation and growth. The temperature was increased from 90 ^{o}C to 250 ^{o}C at rate of 10 ^{o}C/min and then held at 250 ^{o}C for 30 min. After reaction, the product was washed several times with a mixture of hexane and acetone, and then dried in vacuum oven overnight. The resulting product is referred as NW-CNC heterostructures.

2.5. Cyclic Voltammetry Measurement

Cyclic voltammetry (CV) was used to measure the capacitance for NWs, NW-CNT and NW-CNC heterostructures in 9 M, 6 M, 3 M, 1 M, and 0.05 M KOH, respectively. To protect the tip (vycor) of Ag/AgCl reference electrode from being dissolved in base solution, reference electrode was immersed in a saturated KCl solution and using an agar salt bridge to connect two solutions. Platinum wire was used as counter electrode. Copper wires were used as the extent conduct part of working electrode by paste on the back face of sample by silver paint. Insulating paint was used to passivate the back face of working electrode and the exposed part of copper wire. CV measurements were conducted within -1.2 and 0.4 V vs. the Ag/AgCl at different scan rate as 15 mV/s, 30 mV/s, and 50 mV/s, respectively. With each scan rate, CV measurements were repeatedly scanned for 10 times.

2.6. Characterization Methods

Scanning Electron Microscopy (SEM) images Energy-dispersive X-ray Spectra (EDS) were obtained using FE-SEM JEOL-7000 at 20 kV. Tecnai F-20 was used to collect Transmission Electron Microscopy (TEM) images and EDS line-profiling at 200 kV. TEM samples were prepared by dispersing samples on lacey carbon TEM copper grids purchased from Ted Pella Inc. (Redding, CA). The nanowire/CNT diameter/length and average size of Ni nanoparticles were measured form TEM and SEM images, where more than 200 nanowires/CNTs/nanoparticles were counted and measured. All the measurements were carried out using Adobe Photoshop software. X-ray diffraction (XRD) data of samples were recorded with a Philips diffractometer (XRG 3100, Cu Ka radiation, 35mA and 40 kV). Raman spectra and chemical mapping of samples were acquired using a Bruker Senterra Raman microscope (Bruker Optics Inc. Woodlands, TX) with 785nm laser source at 10-25 mW laser powers and a 50× objective lens. The Raman mapping acquisition conditions were set at 3-5 cm^{-1} spectral resolution in the range of 1500-1800 cm^{-1} with 10 mW laser power. A rectangular grid of 15 µm × 15 µm of the sample surface was chosen and scanned 100 points in full range.

3. Results and discussion

Fig. 1 shows the schematic of the heterostructures fabrication: (A) Electrodeposition of Au/Ni multi-segment nanowires using AAO as template. (B) Growth of multi-walled CNTs in a CVD growth, where Ni nanowires acted as catalysts and AAO as a template. This results in NW-CNT heterostructures after the removal of AAO template. (C) Decoration of Ni nanoparticles on NW-CNT heterostructures in a direct wet-chemical method resulting in Au-Ni nanowires-CNT-Ni nanoparticles heterostructures or NW-CNC heterostructures.

Fig. 2 shows the XRD patterns for Au-Ni nanowires, NW-CNT heterostructures, and NW-CNC heterostructures. The as-synthesized Au/Ni nanowires exhibit Au peak and strong peaks of Ni (A in Fig. 2). Nickel exhibited (220), (111), (200), and (311) fcc crystal planes. Au (400) fcc planes were observed for Au-Ni nanowires. The presence of these planes could be attributed to the electrodeposition process [18,19]. After CNT growth (B in Fig. 2), CNT (002) peak was observed [20] as well as Ni_3C (006) and Ni_xC (009) peaks suggested the catalytic Ni after poisoning during the CVD growth process [21]. After the decoration of Ni nanoparticles on NW-CNT heterostructure, the XRD intensity for Ni (111) peak was strengthened indicating low energy faceted growth of Ni nanoparticles (C in Fig. 2). Other peaks for Au, Ni, and CNTs were also observed for NW-CNC heterostructure samples. Fig. 3A and B shows the SEM image of well-aligned Au/Ni nanowires over large area after being released from AAO template. The EDS spectra (Fig. 3A, inset) clearly shows the presence of Ni and Au in the multi-segment nanowires. The interface between the Au segment and the Ni segment is also shown in Fig. 3C. Previously [22,23], multi-segment Ni-Au-Ni nanowires were studied for selective protein tagging and nano-resistor applications.

After the electrodeposition of Au-Ni nanowires, multi-walled CNTs were grown on tips of Ni nanowire segment while inside AAO template. Fig. 4A shows the free-standing NW-CNT heterostructures after the removal of AAO template. Each segment of NW-CNT heterostructures was characterized by SEM and EDS (Fig. 4B and D). Ni nanowires segments acted as catalysts to assist the growth of CNTs in a CVD process. Fig. 4C and E clearly show the presence of Ni nanoparticles at the tips of CNTs indicating tip growth mechanism for the latter [24]. Nanowires and CNTs were well connected after the CVD growth as shown by the interfaces at the junction

(Fig. 4F). However, for several heterostructures, it was noticed that some Au segments and Ni segments were disconnected after the CVD process (Fig. 4G). This may be attributed to recrystallization of Ni or Au nanowires during high temperature CVD process [19,25]. HR-TEM and EDS line profiling method were used to characterize NW-CNT heterostructure interfaces (Fig. 5). HRTEM shows the ~0.34 nm inter-layer spacing for CNTs suggesting a graphitic structure [17]. In addition, it is also possible to see the interface with Ni nanowire segment, where the graphitic carbon is grown parallel to the Ni nanowire tip and then leading into the CNT hollow core. This suggests that layered graphitic carbon formation took place at the interface, which was later continued via tip-growth mechanism carrying the initiator Ni nanoparticle along the growing CNT tip. The EDS line-profiling of NW-CNT heterostructure interface showed that not only the tips of CNTs contain Ni, but there was Ni diffusion across the CNT length as seen by EDS line profile [17]. Furthermore, the NW-CNT heterostructures were characterized by Raman spectroscopy. Fig. 6 showed a typical Raman spectrum of NW-CNT heterostructures and a chemical mapping for G-band of CNTs for a larger area of standing heterostructures with CNTs facing the incident Raman laser. The peaks for graphite structure including D-, G-, and 2D-band were clearly observed in the Raman spectrum.

Fig. 7 represented SEM images and EDS for NW-CNC heterostructures. It can be observed that even after the wet-chemical nucleation process, the heterostructures remain vertically-aligned or standing on the substrate. The EDS analysis shows the presence of various elements on the heterostructures with strong presence of Ni in different regions (Fig. 7B and D). This indicate that Ni was nucleated on all the segments of the heterostructures. However, it could be noticed from the SEM images that the nucleation of Ni nanoparticles was mostly observed on the CNT segment

(Fig. 7C, E-G). Ni nanoparticles with diameter ~20 nm were decorated on NW-CNT heterostructures. The presence of nanoparticles majorly on the surface of CNT was observed due to good wettability of hydrophobic CNT segment in oil phase solution for nucleation of Ni nanoparticles (Fig. 7F and G) [17]. TEM and EDS line-profiling for NW-CNC heterostructures are shown in Fig. 8. Consistent with SEM observations, majority of Ni nanoparticles were present on CNT segment of heterostructures (Fig. 8A and B). HR-TEM of decorated Ni nanoparticles (Fig. 8C) indicated that single-crystal Ni nanoparticles were encapsulated in thin polycrystalline NiO shells attributed to air exposure of heterostructures [26]. Furthermore, scanning transmission electron microscopy (STEM) mode EDS line profiles are performed along the diameter of nanoparticle-decorated CNT segments (Fig. 8D-G). This clearly shows the Ni nanoparticle decoration. To differentiate between the signal from Ni nanoparticle (CNT growth catalyst) inside the CNT core and Ni nanoparticles decorated by wet-chemical approach, the line profiles were performed in two different regions of CNTs as shown by Fig. 8D and F. The broad Ni peak (blue color) in Fig. 8E is due to the Ni nanoparticle within the CNT core while Fig. 8G clearly shows the multiple peaks of Ni across the CNT diameter. Uniform peaks of C and O are also observed, where the latter can be attributed to the NiO shell around Ni nanoparticles. The formation of NiO on Ni nanoparticles was further confirmed by Raman shift peaks for longitudinal optical phonon modes (LO, ~546 cm^{-1}) in Raman spectrum for NW-CNC heterostructures (Fig. 9A) [27]. Fig. 9B-D shows the chemical maps of the heterostructures. Knowing the density of nanowires (~8.3×10^{8} cm^{-2}), the length and diameter of nanowires and CNTs, and the diameter of Ni nanoparticles, it was possible to calculate the specific area of Au-Ni nanowires, NW-CNT heterostructures, and NW-CNC heterostructures (Table S1). This shows that the highest surface area is observed for NW-CNT heterostructures and lowest for after decorating with nanoparticles for the case of NW-

CNC heterostructures. The latter could be due to the aggregation of nucleated nanoparticles. These are only rough estimates of surface area and thus, could be lower than actual values and would be a critical factor for applications of such heterostructures such as supercapacitors [28].

The carbon-based active materials that have high surface areas are commonly used in electrochemical double layer capacitors (EDLCs). Another group of electrochemical capacitors (ECs) utilizes fast and reversible surface or near-surface reactions for charge storage, as known as pseudo-capacitors or redox supercapacitors are also combined with EDLCs or battery electrode to form hybrid capacitors. Among various pseudo-capacitor materials nickel oxide is known to be promising [29]. CNTs have proven to be good materials to construct super-capacitor electrodes due to the high conductivity, electrochemical stability and open porosity [30]. So the construction of Au-Ni NWs-CNTs hybrid structures hold potential as capacitors. The Au segment was designed as current collector [10], Ni was selected as pseudo-capacitor materials [31] or catalyst for the growth of CNTs [32], and CNTs would impart double layer characteristics.

The capacitive behavior of an electrode material is generally characterized by cyclic voltammogram (CV). In an ideal electrical double-layer capacitor containing smooth electrodes, its CV current response shows a rectangular mirror image with respect to the zero-current line [33]. When faradic reaction and Ohmic resistance (resulting from electrolyte diffusion within porous electrode) are involved, the rectangular mirror image is no longer maintained [34]. The capacitance can be calculated through following equations [35]:

$$C = \frac{q}{V_f - V_{io}} \qquad (1)$$

$$q = \frac{\int I(V)dV}{v_{scan}} \qquad (2)$$

Where C is capacitance (F), q is quantity of electric charge (C), V_f is final potential, V_{io} is starting potential, $\int I(V)dV$ is the area of CV curve and represents the average, v_{scan} is the potential scan-rate for CV test. The faradic capacitance is due to the Ni^{2+} to Ni^{3+} redox reaction given as [36,37]:

$$NiO + OH^- \leftrightarrow NiOOH + e^- \quad (3)$$

Nickel hydroxides also exist in the Ni^{2+} to Ni^{3+} redox couple in alkaline solution as [34,36]:

$$Ni(OH)_2 + OH^- \leftrightarrow NiOOH + H_2O + e^- \quad (4)$$

A typical CV measurement for NWs, NW-CNT heterostructures, and NW-CNC heterostructures are shown in Fig. 10. Capacitance for each sample at different conditions were calculated and listed in Table S2 (Supporting Information). The capacitance in NWs could be attributed to the presence of thin NiO layer around Ni segments or the metallic segment double layer formation characteristics. However, the oxide layer on Ni segment was indiscernible in electron microscopic characterizations. Generally, a low scan rate, high KOH concentration, and suitable scan range/window can enhance the electron transfer reactions on electrode and thus, resulting in a higher capacitance (Fig. S1 and S2, Table S2 in Supporting Information) [38]. Fig. 11 shows the trends for the specific capacitance for the NWs, NW-CNT heterostructures, and NW-CNC heterostructures. It was observed that specific capacitance decreased with increasing electrolyte concentration, decreasing scan window, and increasing scan rates. The systematic studies performed here are of great value for understanding and developing optimized energy storage devices using such heterostructures. It is also noted that after adding CNT and Ni nanoparticles on the heterostructures, the capacitance was lowered as compared to other samples. This may attributed to two reasons: (1) After CVD growth of CNT and Ni nanoparticles nucleation, some heterojunctions between Au-Ni nanowires were damaged and disconnected as observed in Fig. 4G and Fig. 7G. The disconnection of nanowires would interrupt the current collection step when

those materials were measured with CV. (2) The surface of multi-walled CNTs grown from AAO template by CVD is hydrophobic. The wettability of CNTs would significantly affect the exposed area of electrode thus a hydrophobic surface may reduce the exposed area of electrode with solution [39]. Also, the Ni nanoparticles nucleation step were conducted in oil-phase solution, which may have led to contamination of hydrophobic surfactant species on the heterostructures. The hydrophobic surface would inhibit the redox reaction since the KOH solution cannot properly wet the nanostructures. Thus, the surface wettability of NW-CNT and NW-CNC heterostructures must be tuned in order to achieve higher capacitance values.

4. Conclusions

Vertically-aligned Au-Ni nanowires axially linked with CNTs with uniform diameters and micron-scale lengths were fabricated by combining electro-deposition and CVD methods by using porous alumina or anodized aluminum oxide template (AAO). Furthermore, these NW-CNT heterostructures were integrated with Ni/NiO core/shell nanoparticles in a wet-chemical approach. The diameters of nanowires and CNTs were determined by porous template size and lengths were controlled by varying the duration of electrodeposition and CVD process. The structural, interfacial, morphological characterization was performed using microscopic and spectroscopic methods. Ni segment of Au-Ni nanowires was utilized as a catalyst for the CVD growth of CNTs. However, CVD growth process was observed to result in disconnected Au and Ni segments due to material migration. Overall, the CVD processing for CNT growth and wet-chemical nucleation of nanoparticles did not disturb the vertical alignment of heterostructures. Electrochemical behavior of various heterostructures were studied and compared. NW-CNT heterostructures showed the highest surface area. The specific capacitance of NWs, NW-CNT heterostructures, and

NW-CNC heterostructures was investigated as a function of electrolyte (KOH) concentration, scan rate, and scan voltage range. The highest specific capacitance for Au/Ni NWs was around 6.8×10^7 μF/g. However, the NW-CNT and NW-CNC heterostructures showed highest capacitance of ~4.1×10^7 μF/g and 9.7×10^6 μF/g, respectively. This decrease in specific capacitance as compared to Au/Ni NWs could be attributed to the damaged interfaces for the nanowire segments and the hydrophobicity of CNTs or hydrophobic contamination of heterostructures during wet-chemical nucleation and growth of Ni nanoparticles.

Acknowledgements

This work has been supported by The University of Alabama's Research Grant Committee Award, NSF-REH award through MINT Center, and NSF-EPSCoR RII award. P.S. thanks NSF-REH for the summer internship financial support. The authors also thank the Central Analytical Facility (CAF) for electron microscopy equipment and other centers for providing infrastructure support such as clean room facility and various equipment. N.C. wrote the manuscript and conducted the analysis. The project was conceptualized and designed by N.C. while experiments were done by P.A. and J.W.

References

[1] Hurst SJ, Payne EK, Qin LD, Mirkin CA. Multisegmented one-dimensional nanorods prepared by hard-template synthetic methods. Angew Chem Int Edit 2006;45:2672-92.

[2] Chopra N. Multi-functional and Multi-component Heterostructured One-Dimensional Nanostructures: Advances in Growth, Characterization, and Applications, Materials Technology: Advanced Performance Materials, 2010;25:212-30.

[3] Ou FS, Shaijumon MM, Ajayan PM. Controlled manipulation of giant hybrid inorganic nanowire assemblies. Nano Lett 2008;8:1853-7.

[4] Hinds BJ, Chopra N, Rantell T, Andrews R, Gavalas V, Bachas LG. Aligned multiwalled carbon nanotube membranes. Science 2004;303:62-5.

[5] Andrews R, Jacques D, Rao AM, Derbyshire F, Qian D, Fan X, Dickey EC, Chen J. Continuous production of aligned carbon nanotubes: a step closer to commercial realization. Chem Phys Lett 1999;303:467-74.

[6] Fan SS, Chapline MG, Franklin NR, Tombler TW, Cassell AM, Dai HJ. Self-oriented regular arrays of carbon nanotubes and their field emission properties. Science 1999; 283:512-4.

[7] Hu JT, Ouyang M, Yang PD, Lieber CM. Controlled growth and electrical properties of heterojunctions of carbon nanotubes and silicon nanowires. Nature 1999;399:48-51.

[8] Luo J, Zhu J, Huang Z, Zhang L. Arrays of Ni nanowire/multiwalled carbon nanotube/amorphous carbon nanotube heterojunctions containing Schottky contacts. Appl Phys Lett 2007;90:033114/1-3.

[9] Che GL, Lakshmi BB, Fisher ER, Martin CR. Carbon nanotubule membranes for electrochemical energy storage and production. Nature 1998:393:346-9.

[10] An KH, Kim WS, Park YS, Moon JM, Bae DJ, Lim SC, Lee YS, Lee YH. Electrochemical properties of high-power supercapacitors using single-walled carbon nanotube electrodes. Adv Funct Mater 2001;11:387-92.

[11] Burke A. Ultracapacitors: why, how, and where is the technology. J Power Sources 2000;91:37-50.

[12] Shaijumon MM, Ou FS, Ci LJ, Ajayan PM. Synthesis of hybrid nanowire arrays and their application as high power supercapacitor electrodes. Chem Commun 2008;20:2373-5.

[13] Pandolfo AG, Hollenkamp AF. Carbon properties and their role in supercapacitors. J Power Sources 2006;157:11-27.

[14] Nam KW, Yoon WS, Kim KB. X-ray absorption spectroscopy studies of nickel oxide thin film electrodes for supercapacitors. Electrochim Acta 2002;47:3201-9.

[15] Lee JY, Liang K, An KH, Lee YH. Nickel oxide/carbon nanotubes nanocomposite for electrochemical capacitance. Synthetic Met 2005;150:153-7.

[16] Wang DW, Li F, Cheng HM. Hierarchical porous nickel oxide and carbon as electrode materials for asymmetric supercapacitor. J Power Sources 2008;185:1563-8.

[17] Chopra N, Shi WW, Bansal A. Structural evolution and stability studies of heterostructures comprised of carbon nanotubes decorated with nickel/nickel oxide core/shell nanoparticles. Carbon 2011;49:3645-62.

[18] Sau TK, Rogach AL. Nonspherical Noble Metal Nanoparticles: Colloid-Chemical Synthesis and Morphology Control. Adv Mater 2010;22:1781-804.

[19] Pan H, Sun H, Poh C, Feng YP, Lin JY. Single-crystal growth of metallic nanowires with preferred orientation. Nanotechnology 2005;16:1559-64.

[20] Ci LJ, Wei BQ, Xu CL, Liang J, Wu DH, Xie SS, Zhou WY, Li YB, Liu ZQ, Tang DS. Crystallization behavior of the amorphous carbon nanotubes prepared by the CVD method. J Cryst Growth 2001;233:823-8.

[21] Zhou W, Zheng K, He L, Wang R, Guo L, Chen C, Han X, Zhang Z. Ni/Ni3C core-shell nanochains and its magnetic properties: One-step synthesis at low temperature. Nano Lett 2008;8:1147-52.

[22] Lee KB, Park S, Mirkin CA. Multicomponent magnetic nanorods for biomolecular separations. Angew Chem Int Edit 2004;43:3048-50.

[23] Hangarter CM, Myung NV. Magnetic alignment of nanowires. Chem Mater 2005;17:1320-24.

[24] Han JH, Yoo JB, Park CY, Kim HJ, Park GS, Yang M, Han IT, Lee N, Yi WK, Yu SG, Kim JM. Tip growth model of carbon tubules grown on the glass substrate by plasma enhanced chemical vapor deposition. J Appl Phys 2002;91:483-6.

[25] Luton MJ, Sellars CM. Dynamic recrystallization in nickel and nickel-iron alloys during high temperature deformation. Acta Metall Mater 1969;17:1033-43.

[26] Xia X, Tu J, Wang X, Gu C, Zhao X. Hierarchically porous NiO film grown by chemical bath deposition via a colloidal crystal template as an electrochemical pseudocapacitor material. J Mater Chem 2011;21:671-9.

[27] Wang WZ, Liu YK, Xu CK, Zheng CL, Wang GH. Synthesis of NiO nanorods by a novel simple precursor thermal decomposition approach. Chem Phys Lett 2002;362:119-22.

[28] Simon P, Gogotsi Y. Materials for electrochemical capacitors. Nat Mater 2008;7:845-54.

[29] Lang JW, Kong LB, Wu WJ, Luo YC, Kang L. Facile approach to prepare loose-packed NiO nano-flakes materials for supercapacitors. Chemical Communications 2008;35:4213-5.

[30] Futaba DN, Hata K, Yamada T, Hiraoka T, Hayamizu Y, Kakudate Y, Tanaike O, Hatori H, Yumura M, Iijima S. Shape-engineerable and highly densely packed single-walled carbon nanotubes and their application as super-capacitor electrodes. Nat Mater 2006;5:987-94.

[31] Yuan GH, Jiang ZH, Aramata A, Gao YZ. Electrochemical behavior of activated-carbon capacitor material loaded with nickel oxide. Carbon 2005;43:2913-7.

[32] Luo J, Zhang L, Zhang YJ, Zhu J. Controlled growth of one-dimensional metal-semiconductor and metal-carbon nanotube heterojunctions. Adv Mater 2002;14:1413-4.

[33] Yoon S, Lee JW, Hyeon T, Oh SM. Electric double-layer capacitor performance of a new mesoporous carbon. J Electrochem Soc 2000;147:2507-12.

[34] Wu MS, Hsieh HH. Nickel oxide/hydroxide nanoplatelets synthesized by chemical precipitation for electrochemical capacitors. Electrochim Acta 2008;53:3427-35.

[35] Srinivasan V, Weidner JW. Studies on the capacitance of nickel oxide films: Effect of heating temperature and electrolyte concentration. J Electrochem Soc 2000;147:880-5.

[36] Hsieh CT, Chou YW, Chen WY. Synthesis and electrochemical characterization of carbon nanotubes decorated with nickel nanoparticles for use as an electrochemical capacitor. J Solid State Electr 2008;12:663-9.

[37] Srinivasan V, Weidner JW. An electrochemical route for making porous nickel oxide electrochemical capacitors. J Electrochim Soc 1997;144:L210-3.

[38] Nicholson RS. Theory and application of cyclic voltammetry for measurement of electrode reaction kinetics. Anal Chem 1965;37:1351-5.

[39] Shi W, Venkatachalam K, Gavalas V, Qian D, Andrews R, Bachas LG, Chopra N. The role of plasma treatment on electrochemical capacitance of undoped and nitrogen doped carbon nanotubes. Nanomaterials and Energy 2013;2:71-81.

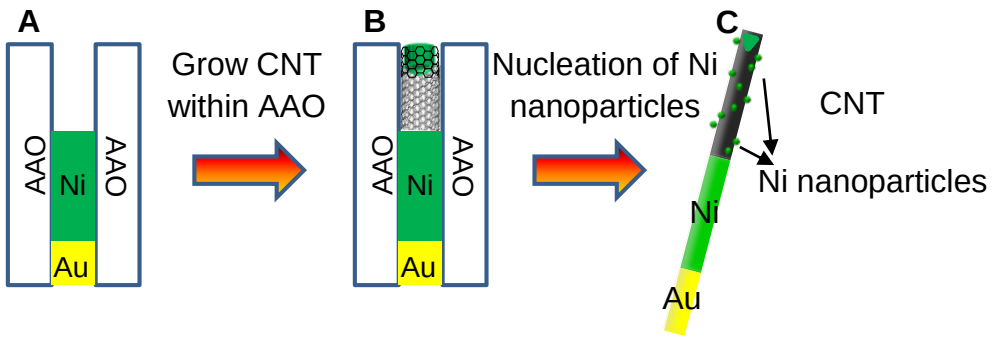

Fig. 1 - Schematic illustrating (A) Electrodeposition of Au/Ni nanowire, (B) growth of CNT on tip of nanowire in a CVD process, and (C) decoration of Ni/NiO core/shell nanoparticles on NW-CNT heterostructure in a wet-chemical approach.

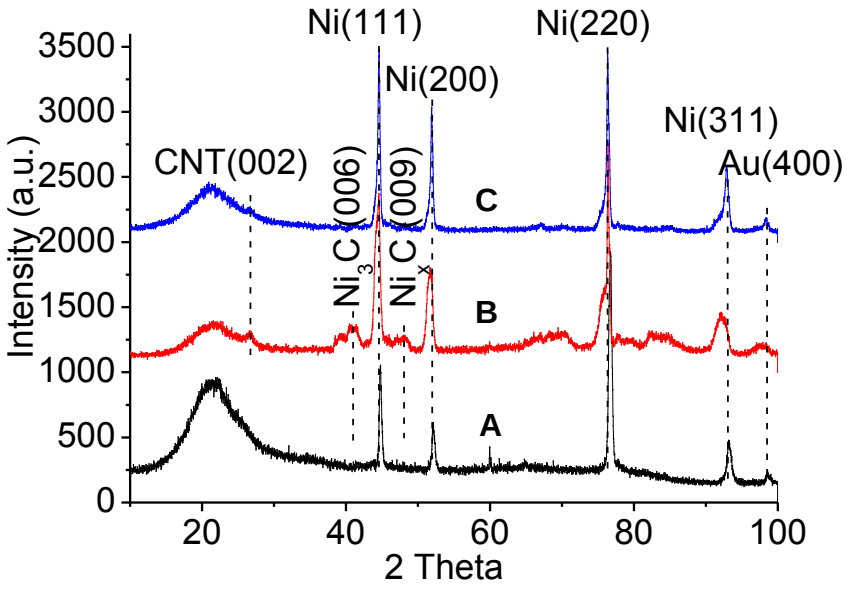

Fig. 2 - XRD of (A) Au/Ni NWs, (B) NW-CNT heterostructures, and (C) NW-CNC heterostructures.

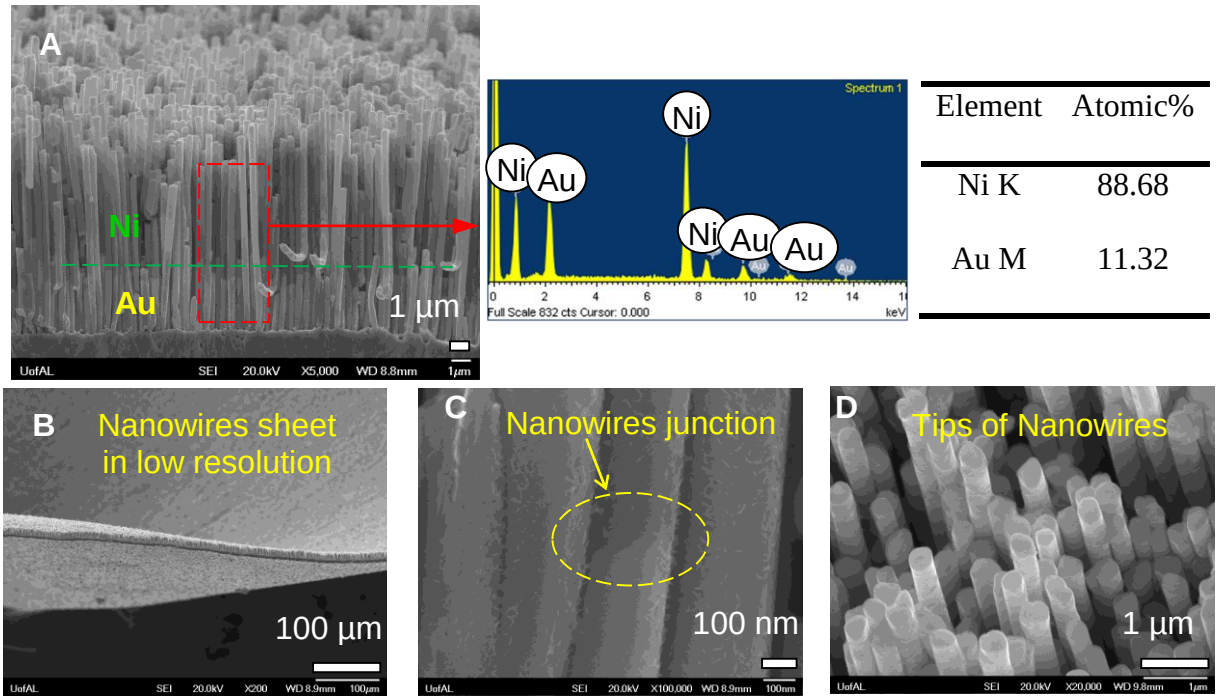

Element	Atomic%
Ni K	88.68
Au M	11.32

Fig. 3 – (A) SEM image of vertically-aligned Au/Ni NWs with EDS showing elemental composition. (B) SEM image showing the Au/Ni NWs over a large area after releasing from porous template. (C) Nanowire heterojunctions and (D) tips,

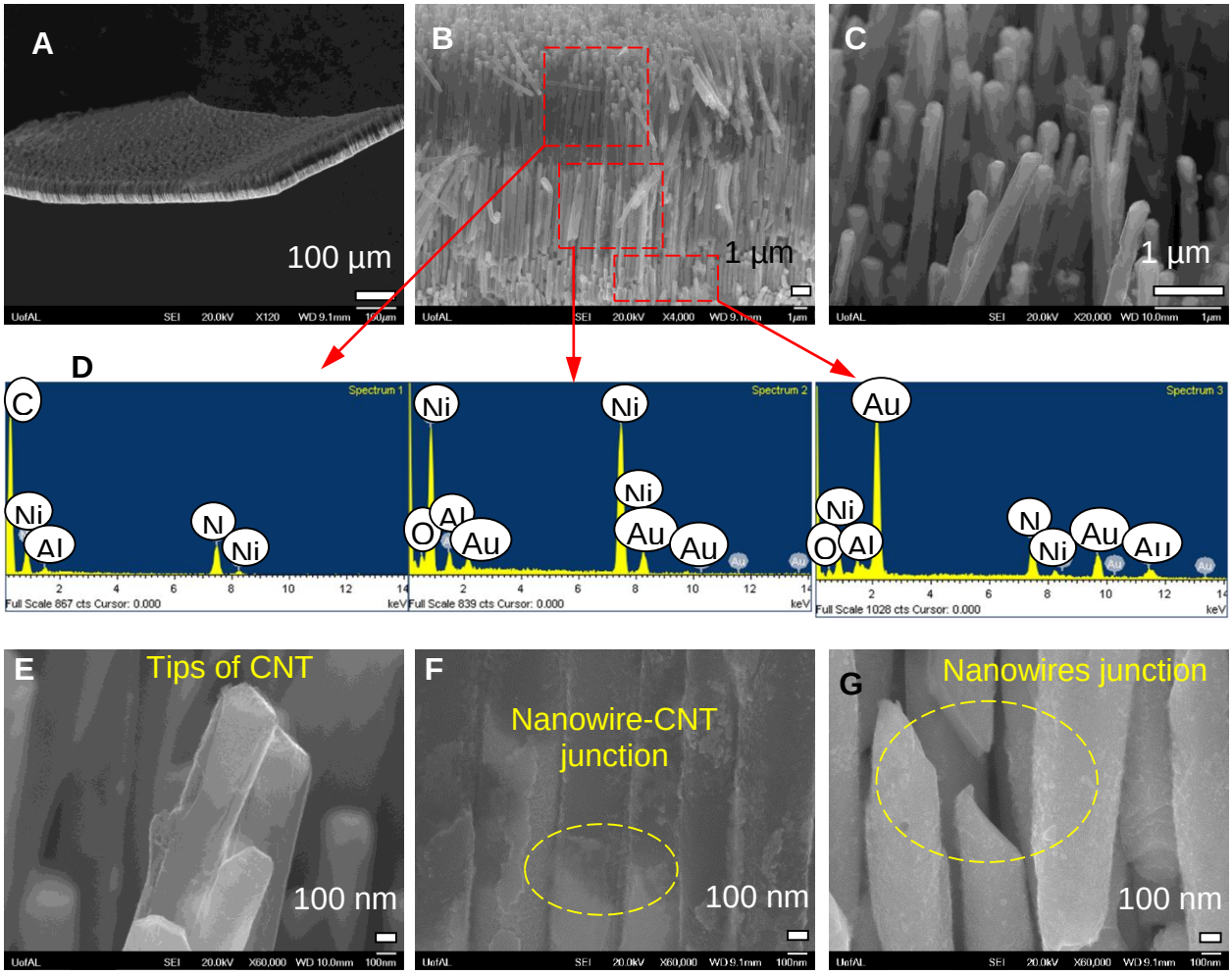

Fig. 4 - SEM images and EDS for NW-CNT heterostructures. (A) vertically-aligned array of NW-CNT heterostructures over a large area substrate after released from porous template. (B) Various segments of heterostructures analyzed using EDS. (C) CNT segment for the array shown in (A). (E) CNT tips with catalyst Ni nanoparticle within the core. (F) Ni nanowire segment and CNT junctions. (G) Disconnected nanowire segments after the CVD growth process.

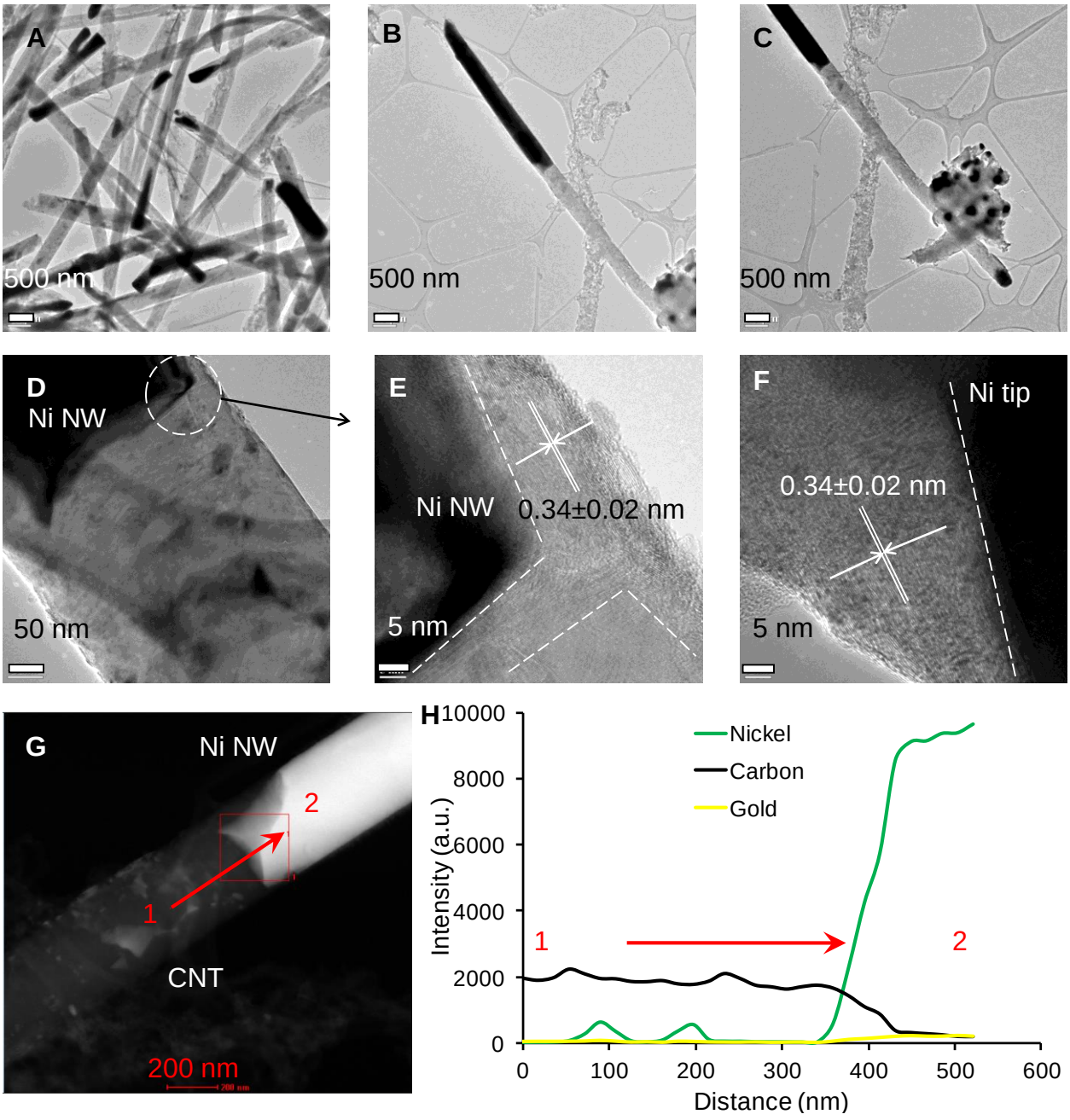

Fig. 5 - (A-F) TEM images showing the morphology, structure, and interface for NW-CNT heterostructures, (G and H) STEM mode EDS line profile showing NW-CNT heterostructure. The red arrow indicate the direction of line profiling scan and the location.

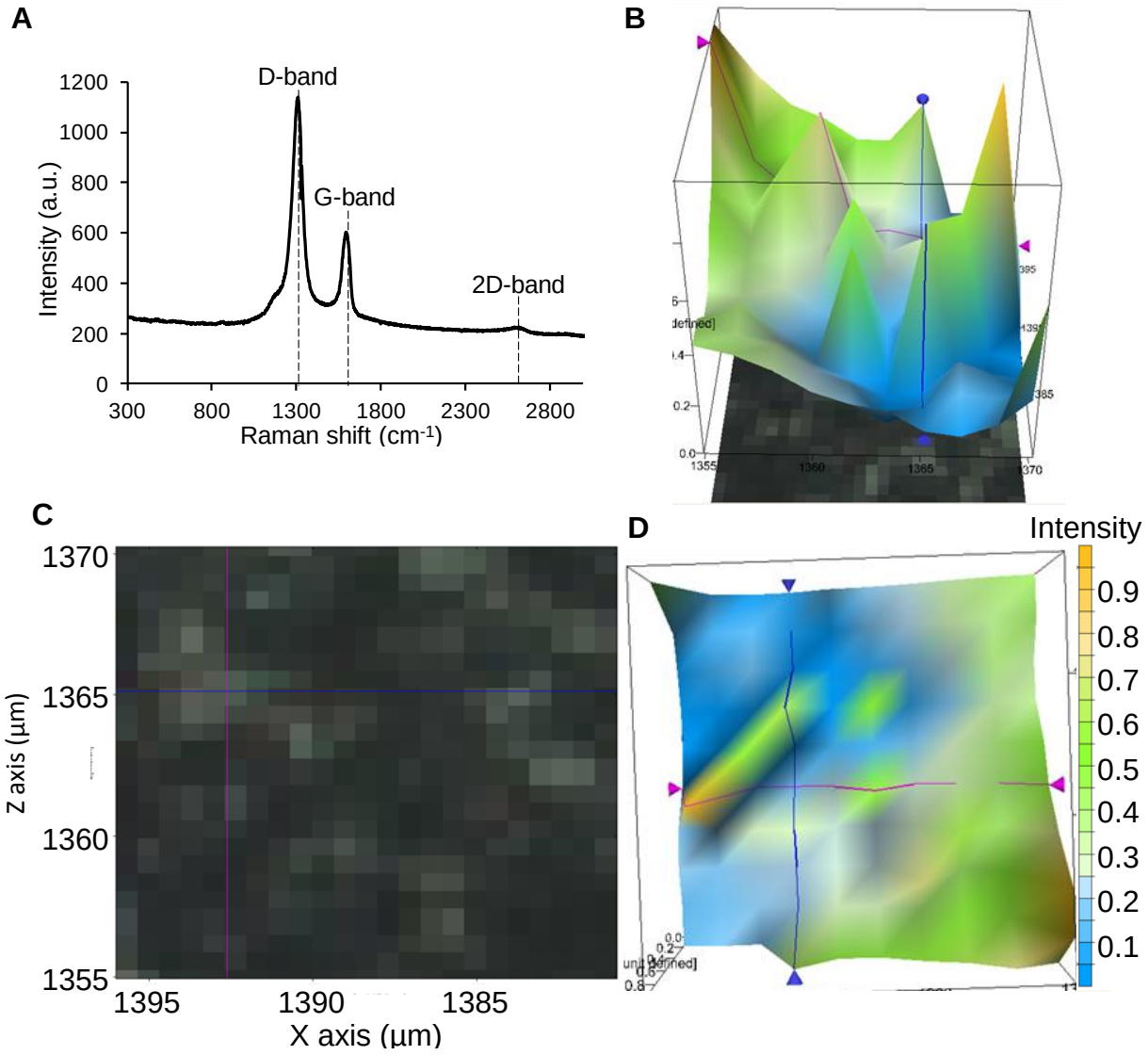

Fig. 6 - (A) Raman spectrum of NW-CNT heterostructures. (B) 3D chemical mapping for G-band for the heterostructures. (C) Optical image at 100x magnification showing sample surface. (D) Vertical view of Raman 3D chemical map.

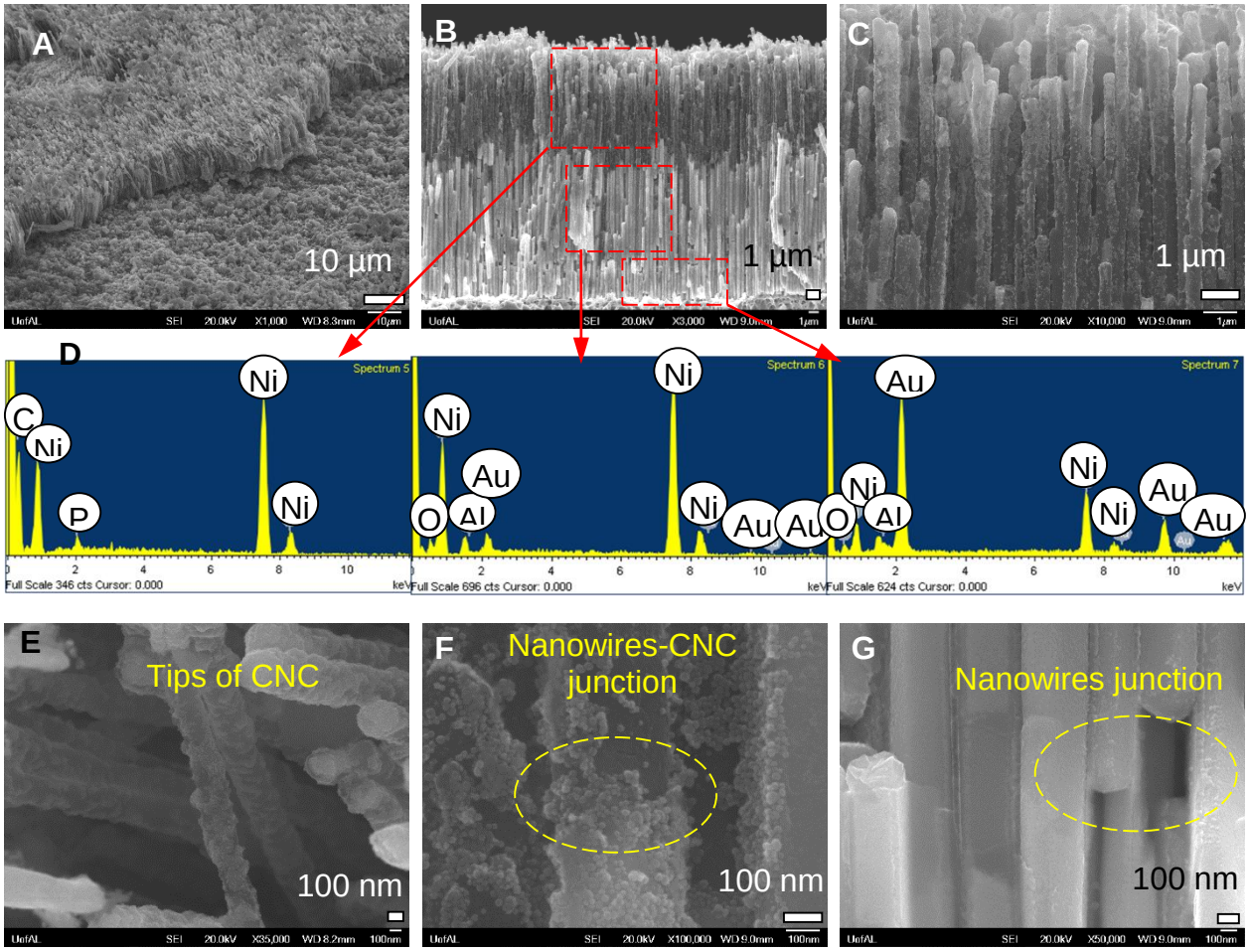

Fig. 7 - (A-C) SEM images of NW-CNC heterostructures. (D) EDS for different segment of heterostructures, and SEM for (E) CNT tips decorated with nanoparticles, (F) heterojunctions for CNT and nanowire segments, and (G) Au-Ni nanowires junctions with some disconnected segments.

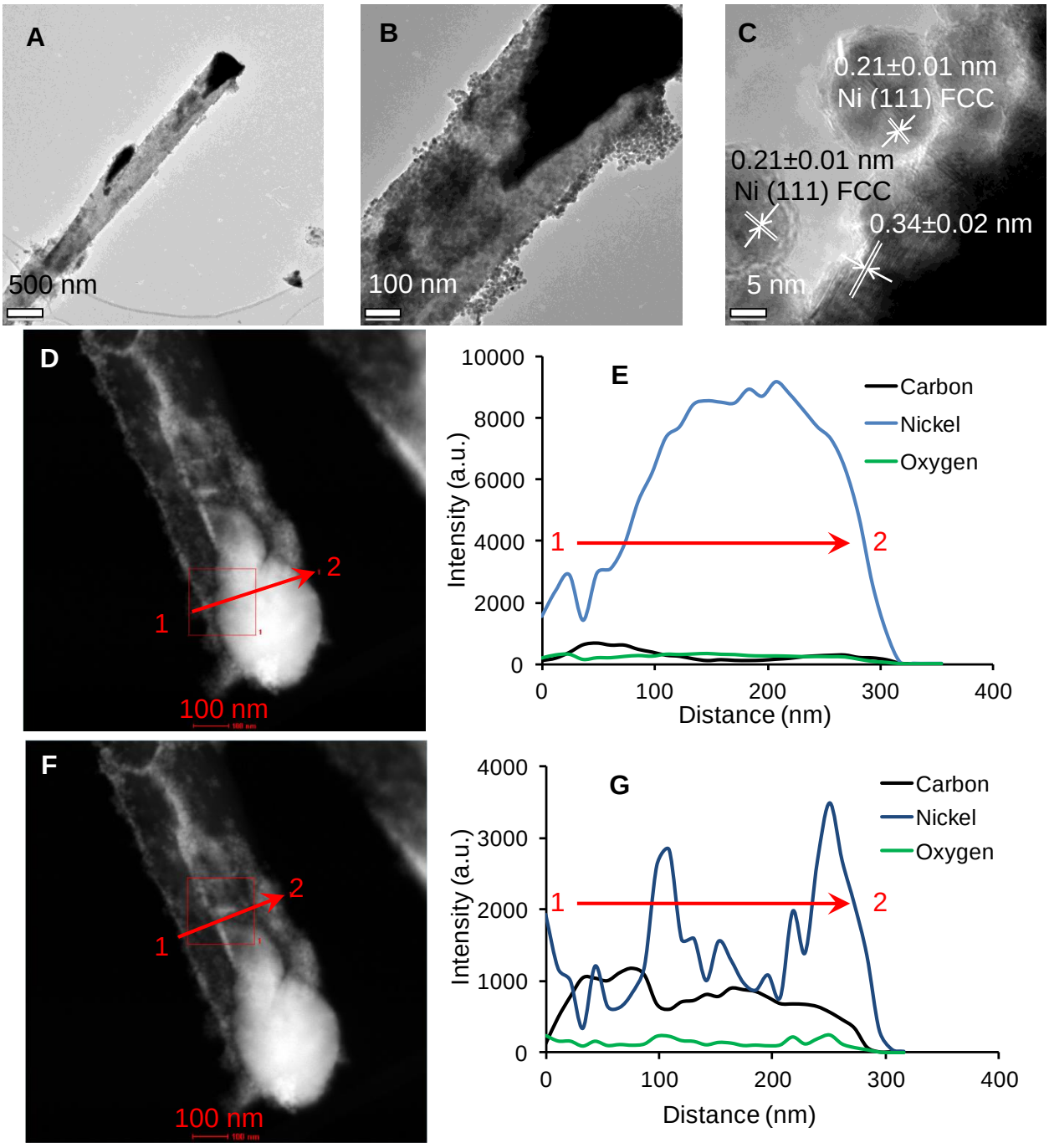

Fig. 8 - (A-C) TEM images showing NW-CNC heterostructures, (B) shows the CNT tip with catalyst Ni nanoparticle within the core and decorated with Ni/NiO core.shell nanoparticles on the external surface. (C) Core/shell structure of the decorated nanoparticles. (D-G) STEM mode EDS line profile for nanoparticle-decorated CNT tip and other section of the same CNT.

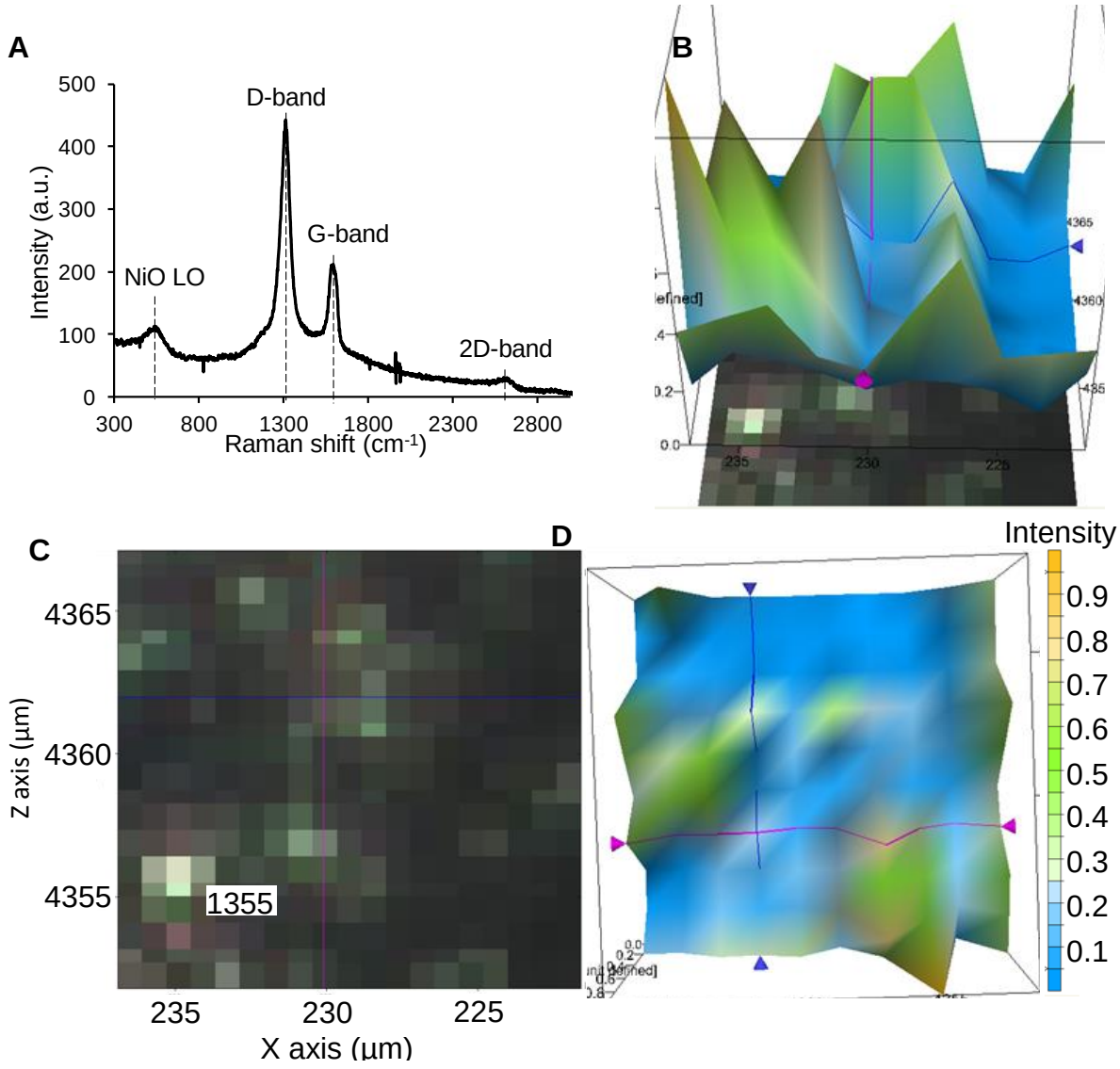

Fig. 9 - (A) Raman spectrum for NW-CNC heterostructures. (B) 3D chemical mapping for G-band intensity for NW-CNC heterostructures. (C) Optical image at 100x magnification for sample surface. (D) Vertical view of 3D chemical map.

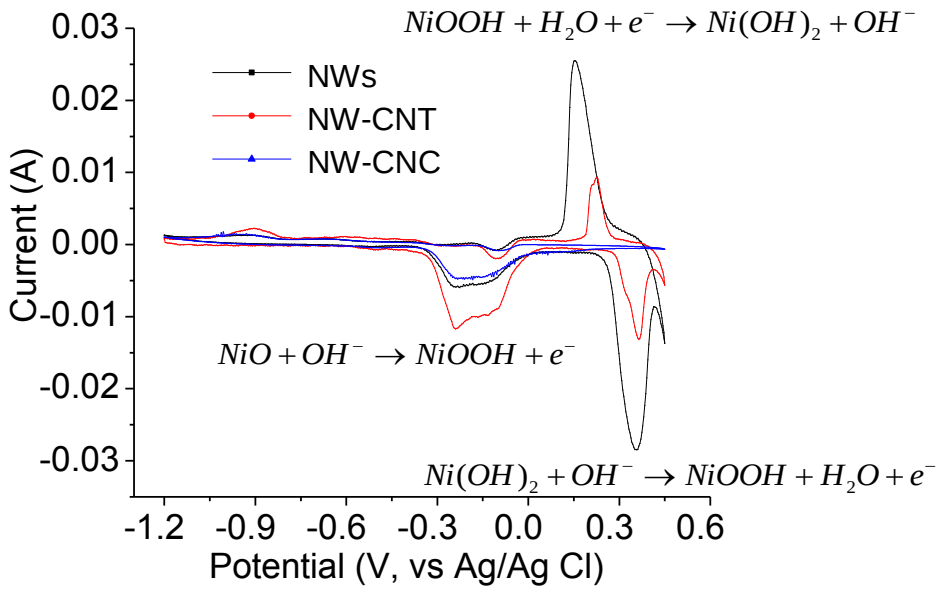

Fig. 10. A representative cyclic voltammetric (CV) measurements for NWs, NW-CNT heterostructures, and NW-CNC heterostructures in 9 M KOH solution with scan rate of 30 mV/s.

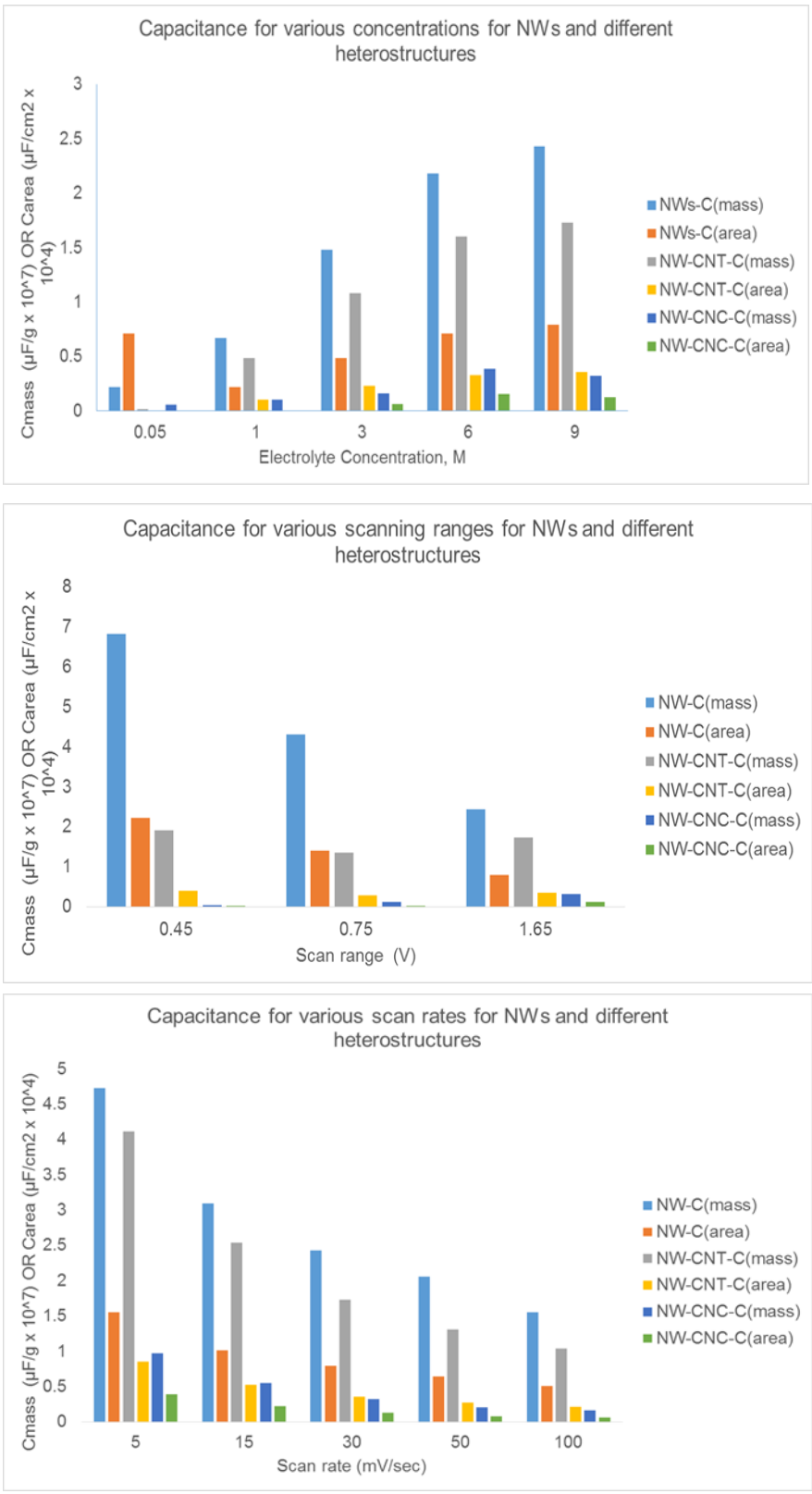

Fig. 11. Specific capacitance vs. electrolyte concentration, scan range, and scan rate for various samples (NWs, NW-CNT heterostructures, and NW-CNC heterostructures). The capacitance values correspond to w.r.t mass (C_{mass}) and area (C_{area}).

Supporting Information for

Synthesis of nanoscale heterostructures comprised of metal nanowires, carbon nanotubes, and metal nanoparticles: Investigation of their structure and electrochemical properties

Nitin Chopra,[1,2,*] Junchi Wu,[1] Paaras Agrawal[3]

[1] *Metallurgical and Materials Engineering, Center for Materials for Information Technology (MINT), Box 870202, The University of Alabama, Tuscaloosa, AL 35401 USA*

[2] *Department of Biological Sciences, Box 870202, The University of Alabama, Tuscaloosa, AL 35401 USA*

[3] *NSF-REH, Northridge High School, 2901 Northridge Rd, Tuscaloosa, AL 35406 USA*

[*] Corresponding author. Tel: 205-348-4153; Fax: 205-348-2164; E-mail: nchopra@eng.ua.edu (N. Chopra)

Table S1 - Surface area estimated for NWs, NW-CNT heterostructures, and NW-CNC heterostructures based on SEM and TEM images.

	NWs	NW-CNT heterostructures	NW-CNC heterostructure
Piece area (cm^2)	0.24	0.2	0.21
Surface area (cm^2)	19.60	29.92	31.49
Surface area per unit sample area	82	150	150
Surface area per mass (cm^2/g)	3062.5	4825.8	2624.2

Table S2 – Specific capacitances estimated for NWs, NW-CNT heterostructures, and NW-CNC heterostructures as a function of electrolyte concentration (KOH), scan ranges, and scan rates.

Sample	Mass (g)	Concentration of KOH (M)	Scan range (V vs. Ag/AgCl)	Scan Rate (mV/s)	C(μF)	C_{mass} (μF/g)	C_{area} (μF/cm^2)
NWs	0.0064	9M	-1.2-0.45	100	9.94×10^4	1.55×10^7	5.07×10^3
			-1.2-0.45	50	1.32×10^5	2.06×10^7	6.47×10^3
			-1.2-0.45	30	1.56×10^5	2.43×10^7	7.93×10^3
			-0.3~0.45	30	2.76×10^5	4.31×10^7	1.41×10^4
			0~0.45	30	4.37×10^5	6.83×10^7	2.23×10^4
			-1.2-0.45	15	1.98×10^5	3.09×10^7	1.01×10^4
			-1.2-0.45	5	3.03×10^5	4.73×10^7	1.55×10^4
		6M	-1.2-0.45	30	1.39×10^5	2.18×10^7	7.11×10^3
		3M	-1.2-0.45	30	9.49×10^4	1.48×10^7	4.84×10^3
		1M	-1.1-0.45	30	4.30×10^4	6.72×10^6	2.19×10^3
		0.05M	-1.1-0.45	30	1.39×10^4	2.17×10^6	7.10×10^2
NW-CNT heterostructures	0.0062	9M	-1.2-0.45	100	6.42×10^4	1.04×10^7	2.15×10^3
			-1.2-0.45	50	8.12×10^4	1.31×10^7	2.71×10^3
			-1.2-0.45	30	1.07×10^5	1.73×10^7	3.58×10^3
			-0.3~0.45	30	8.44×10^4	1.36×10^7	2.82×10^3
			0~0.45	30	1.19×10^5	1.91×10^7	3.96×10^3
			-1.2-0.45	15	1.58×10^5	2.54×10^7	5.27×10^3
			-1.2-0.45	5	2.55×10^5	4.11×10^7	8.52×10^3
		6M	-1.2-0.45	30	9.90×10^4	1.60×10^7	3.31×10^3
		3M	-1.2-0.45	30	6.67×10^4	1.08×10^7	2.31×10^3
		1M	-1.1-0.45	30	3.01×10^4	4.86×10^6	1.00×10^3
		0.05M	-1.1-0.45	30	1.05×10^3	1.7×10^5	30
NW-CNC heterostructures	0.0125	9M	-1.2-0.45	100	2.00×10^4	1.60×10^6	6.30×10^2
			-1.2-0.45	50	2.55×10^4	2.03×10^6	8.10×10^2
			-1.2-0.45	30	4.04×10^4	3.23×10^6	1.28×10^3
			-0.3~0.45	30	1.45×10^3	1.20×10^5	50
			0~0.45	30	4.05×10^3	3.20×10^5	1.30×10^2
			-1.2-0.45	15	6.87×10^4	5.49×10^6	2.19×10^3
			-1.2-0.45	5	1.21×10^5	9.70×10^6	3.87×10^3
		6M	-1.2-0.45	30	4.85×10^4	3.88×10^6	1.52×10^3
		3M	-1.2-0.45	30	2.02×10^4	1.61×10^6	6.40×10^2
		1M	-1.1-0.45	30	1.30×10^4	1.04×10^6	40
		0.05M	-1.1-0.45	30	7.13×10^3	5.7×10^5	20

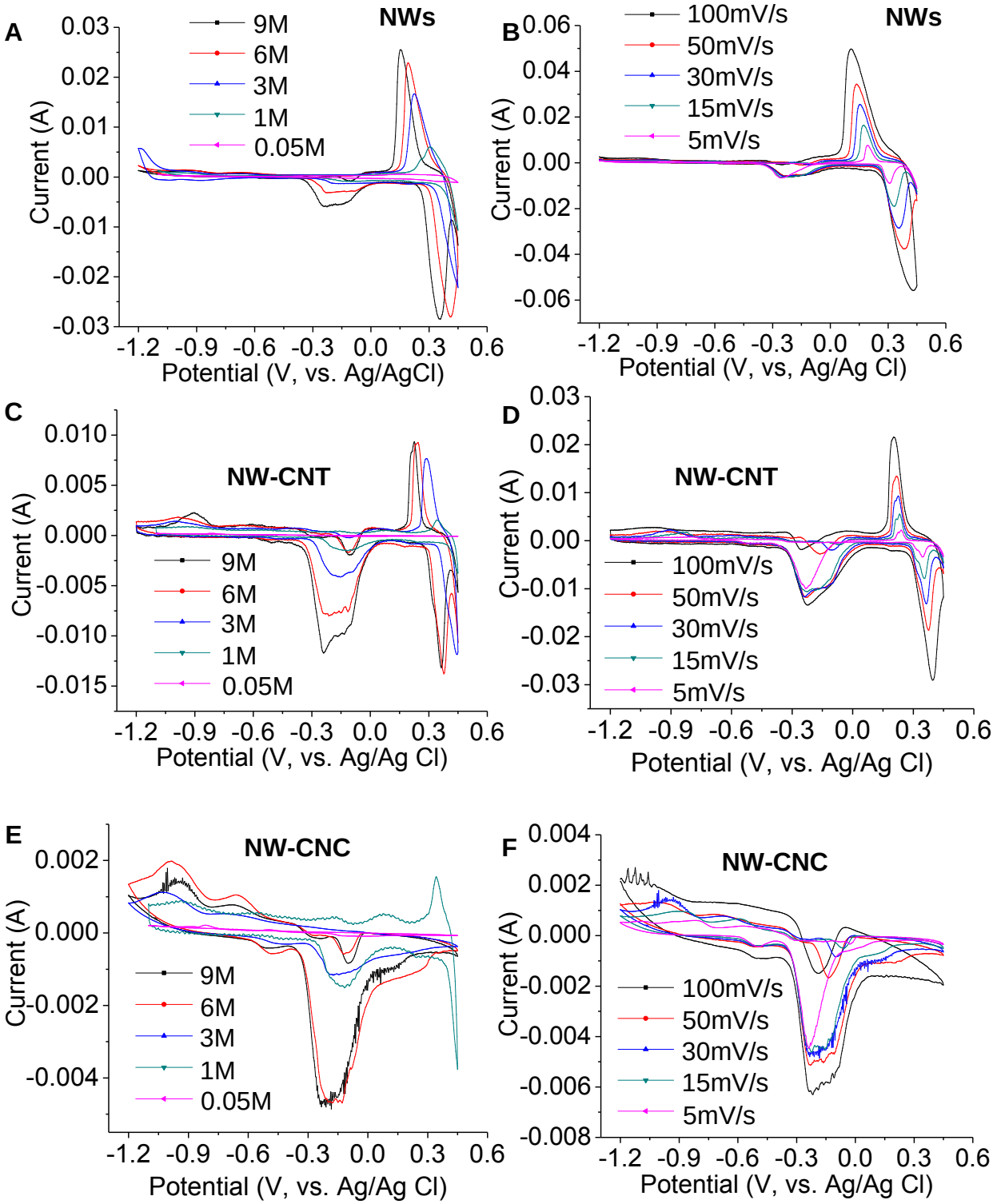

Fig. S1 - CV measurements for (A, B) NWs, (C, D) NW-CNT heterosructures, and (E, F) NW-CNC heterostructures at (A, C, E) different concentrations of KOH solution and (B, D, F) different scan rates.

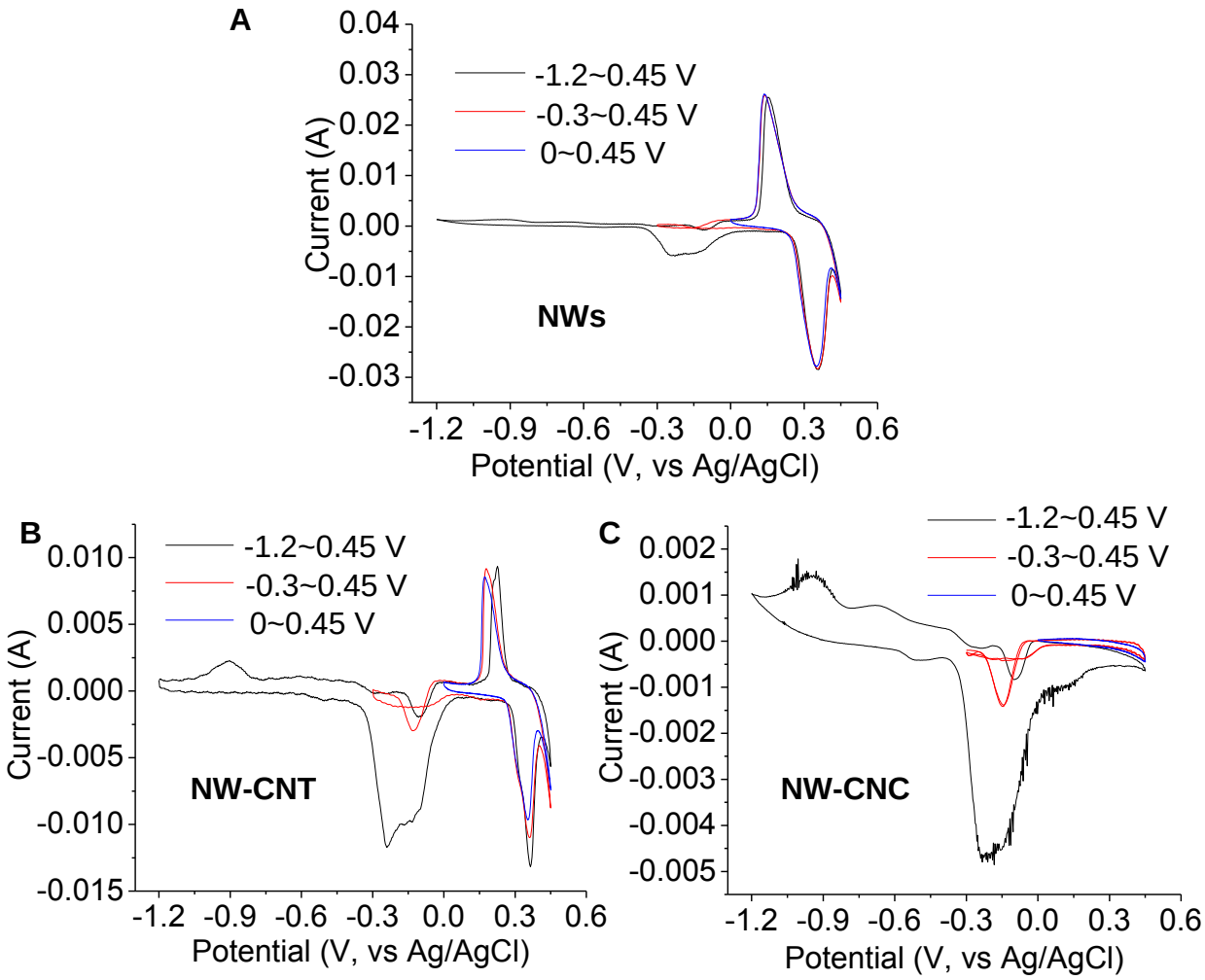

Fig. S2 - CV measurements for (A) NWs, (B) NW-CNT heterostructures, and (C) NW-CNC heterostructures at different scanning windows